Research on the influence of flexible wheelset rotation effect on wheel rail contact force

Lixia Sun, Yuanwu Cai, Di Cheng, Xiaoyi Hu and Chunyang Zhou

Railway Science and Technology Research and Development Center,
China Academy of Railway Sciences Corporation Limited, Beijing, China

Abstract

Purpose – Under the high-speed operating conditions, the effects of wheelset elastic deformation on the wheel rail dynamic forces will become more notable compared to the low-speed condition. In order to meet different analysis requirements and selecting appropriate models to analyzing the wheel rail interaction, it is crucial to understand the influence of wheelset flexibility on the wheel-rail dynamics under different speeds and track excitations condition.

Design/methodology/approach – The wheel rail contact points solving method and vehicle dynamics equations considering wheelset flexibility in the trajectory body coordinate system were investigated in this paper. As for the wheel-rail contact forces, which is a particular force element in vehicle multibody system, a method for calculating the Jacobian matrix of the wheel-rail contact force is proposed to better couple the wheel-rail contact force calculation with the vehicle dynamics response calculation. Based on the flexible wheelset modeling approach in this paper, two vehicle dynamic models considering the wheelset as both elastic and rigid bodies are established, two kinds of track excitations, namely normal measured track irregularities and short-wave irregularities are used, wheel-rail geometric contact characteristic and wheel-rail contact forces in both time and frequency domains are compared with the two models in order to study the influence of flexible wheelset rotation effect on wheel rail contact force.

Findings – Under normal track irregularity excitations, the amplitudes of vertical, longitudinal and lateral forces computed by the flexible wheelset model are smaller than those of the rigid wheelset model, and the virtual penetration and equivalent contact patch are also slightly smaller. For the flexible wheelset model, the wheel rail longitudinal and lateral creepages will also decrease. The higher the vehicle speed, the larger the differences in wheel-rail forces computed by the flexible and rigid wheelset model. Under track short-wave irregularity excitations, the vertical force amplitude computed by the flexible wheelset is also smaller than that of the rigid wheelset. However, unlike the excitation case of measured track irregularity, under short-wave excitations, for the speed within the range of 200 to 350 km/h, the difference in the amplitude of the vertical force between the flexible and rigid wheelset models gradually decreases as the speed increase. This is partly due to the contribution of wheelset's elastic vibration under short-wave excitations. For low-frequency wheel-rail force analysis problems at speeds of 350 km/h and above, as well as high-frequency wheel-rail interaction analysis problems under various speed conditions, the flexible wheelset model will give results agrees better with the reality.

Originality/value – This study provides reference for the modeling method of the flexible wheelset and the coupling method of wheel-rail contact force to the vehicle multibody dynamics system. Furthermore, by comparative research, the influence of wheelset flexibility and rotation on wheel-rail dynamic behavior are obtained, which is useful to the application scope of rigid and flexible wheelset models.

Keywords Flexible wheelset, Contact points calculation, Rotational effects, Elastic modes, Wheel-rail force

Paper type Research paper

1. Introduction

There is a trend towards higher speeds for high speed trains, which will lead to the rapidly increases of wheelsets angular velocity and flexible wheelset rotation effect. Theoretically, wheelset elastic deformation on wheel rail interaction will become more notable at higher speeds compared to lower speeds condition. Especially in cases where short-wave irregularities or defects exist on the wheel-rail interface, the dynamic interaction mechanism between wheels and rails becomes more complex, more appropriate methods and detailed models of vehicle dynamics may be necessary. In view of this, the researches both at home and abroad have established wheelset flexible model to study the influence of wheelset elastic deformation on the dynamic interaction between wheel and rail, as well as on the vehicle's dynamic behavior. Findings indicate that wheelset elastic deformation not only affects the high-frequency dynamic behavior of the vehicle, but also the low-frequency dynamic performance.

In the present study, Cui, Yao, Hu, Sun, and Chang (2019) and Zhong and Jin (2017) considered the wheelset as a rotating elastic body, analyzed the characteristics of wheel-rail forces under the influence of wheelset rotation effects. Their research revealed that the vertical force fluctuation of the flexible wheelset on the wheel-rail interface exhibits multiple dominant frequencies when considering rotational effects. Moreover, a frequency separation phenomenon occurs in the natural frequencies of the wheelset, and as the rotational speed of the wheelset increases, this frequency separation phenomenon becomes more obvious. Baeza, Fayos, Roda, and Insa (2008) considered the presence of wheel flat, the most important conclusion of the wheel flat calculations is that the rigid wheelset model overestimates the peak wheel–rail contact force. The effects of flexible wheelset on the dynamic response are illustrated considering different vehicle speeds and sizes of the wheel flat (Wu, Rakheja, Ahmed, & Chi, 2018), the results show that the flexible wheelset lead to higher axle-box vibration and axle stress compared to a rigid wheelset in the presence of a wheel flat, while revealed slightly lower magnitudes of wheel–rail contact force compared to the rigid wheelset, that is also proved by the study of Momhur (Momhur, Zhao, Quan, Sun, & Zou, 2021). Song *et al.* (2018) and Ma *et al.* (2021) have studied the wheel rail vibration characteristics in the case of rail corrugation. The research by Song *et al.* (2018) shows that modal resonance will cause greater amplitude of vibration of the flexible body than that of the rigid body, while the amplitude of vibration of the flexible body will be smaller than that of rigid body when the modal resonance is far away. Ma *et al.* (2021) find that the wheelset flexibility has limited influence on vertical force resonances but significant contribution to friction power resonances.

In addition to rail corrugation and wheel flat, an increasing number of studies (Han *et al.*, 2018; Hu, Hou, Song, Cheng, & Hou, 2018; Sun, Ai, Gao, Zhang, & Cui, 2023) suggest that for the research on wheel polygons, considering both the wheel and rail as flexible get more realistic simulation results. Sun *et al.* (2023) compared the rail accelerations calculated by flexible and rigid polygons wheelset models, the rail acceleration amplitude is amplified at the wheelset polygons excitation frequency and its half frequency, this may lead to a deterioration of the track components vibration and great attention should be paid.

In addition to the high-frequency dynamic behavior, the influence of wheelset elastic deformation on low-frequency dynamic performance has also been investigated. Research by Casanueva, Alonso, Eziolaza, and Jose (2014) found that the bending modes of the flexible wheelset can affect the critical speed and stability of vehicle, the antisymmetric bending mode shapes will affect the dynamic stability while the influence of the symmetric bending mode shapes is negligible. Comparisons of wheel-rail contact parameters between the flexible wheelset and the rigid wheelset were compared in the study of Zhang, Lu, and Wang, (2013) and Yang and Ren (2018) wheelset's bending deformation was found to have an impact on wheel rail contact locations and contact parameters. Results show that when the wheelset

lateral displacement exceeds 5mm, the wheel rail contact parameters change significantly due to wheelset structural flexibility. Furthermore, Han and Zhang (2015) found in his research that: the wheelset first order bending mode will cause a decrease in the vehicle's critical speed, nevertheless the second and third order bending has little impact on the stability of the vehicle.

Given that the elastic deformation of the wheelset affects the contact geometry parameters and contact behavior between the wheel and rail, this paper suggests a method for solving the wheel rail contact points considering wheelset flexibility, the method of vehicle dynamic equations considering wheelset flexibility in the trajectory body coordinate system is investigated, and a Jacobian matrix calculation method for the wheel-rail contact force is proposed. Both the rigid wheelset model and flexible wheelset model which considers rotational effects are established, the discrepancy in geometric contact characteristics and wheel-rail forces both in time and frequency domain under measured track irregularities and short-wave irregularities are analyzed which aims at further discuss the influence of wheelset flexibility and rotation on vehicle dynamic behavior.

2. Approaches and methods of wheel rail contact algorithm for flexible wheelset
When considering the elastic deformation of the wheelset, at each time step of wheel-rail contact force calculation, elastic deformation should be considered, which mainly involved the solution of geometric contact, wheel-rail contact force and how to get the equivalent force on the node. The computational methods will be discussed what follows in the passage.

2.1 Description of floating coordinate system for arbitrary
The trajectory body coordinate is defined to formulate the equations of motion of vehicle systems, it has an advantage that the position of arbitrary body can be determined easily which is a problem if the track coordinate system is located in the absolute coordinate. Figure 1 illustrates the definition of the trajectory body coordinate system, where three coordinate systems are used that are the global coordinate system $OXYZ$, the trajectory body coordinate system $O^{ti}X^{ti}Y^{ti}Z^{ti}$, and the wheelset body fixed coordinate system $O^{i}X^{i}Y^{i}Z^{i}$. The global coordinate system $OXYZ$ is assumed to be fixed and is used for all bodies to define global vectors, absolute velocities and accelerations.
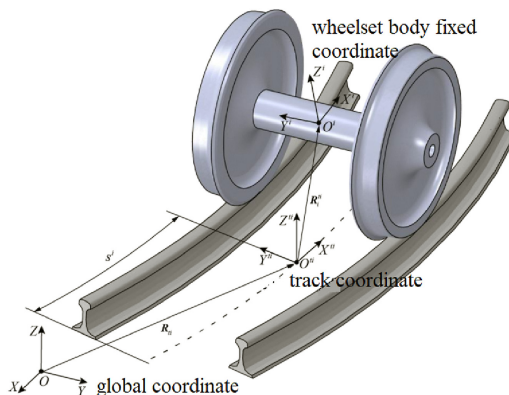
Source(s): Authors' own work

Figure 1.
Trajectory body coordinate system in the global coordinate

The position of the trajectory body coordinate system is determined by the arc length coordinate s^i of body i, the arc length coordinate is defined as the distance traveled by the body along the track. Based on the track geometry data, the trajectory body coordinate system can be uniquely determined in terms of the arc length s^i, including the position $\boldsymbol{R}_{ti}(s^i)$ and Euler angles of the trajectory body coordinate system relative to the global system.

Using the trajectory body coordinate, the global position vector of any point p on body i can be expressed as:

$$\boldsymbol{r}_p^i = \boldsymbol{R}_{ti} + \boldsymbol{A}_{ti}\left(\boldsymbol{R}_i^{ti} + \boldsymbol{A}_i^{ti}\boldsymbol{u}_p^i\right) \tag{1}$$

In equation (1), $\boldsymbol{R}_i^{ti}$ represents the position vector of the origin of the body-fixed coordinate system $O^i X^i Y^i Z^i$ attached to body i relative to the trajectory body coordinate system. $\boldsymbol{u}_p^i$ denotes the position vector of point p in the body-fixed coordinate system of body i. $\boldsymbol{A}_{ti}$ represents the coordinate transformation matrix from the trajectory body coordinate system to the global coordinate system, $\boldsymbol{A}_i^{ti}$ is the transformation matrix from wheelset body-fixed coordinate system to the trajectory body coordinate system, Both the $\boldsymbol{A}_{ti}$ and $\boldsymbol{A}_i^{ti}$ can be expressed by Euler angles, which are not discussed in this paper.

When considering the body's elastic deformation, it is necessary to obtain the posture and position of the body as well as the body deformation. Therefore, modal coordinates which representing the contribution of deformation of the flexible body must be added to Equation (1), it can be represented as follows:

$$\boldsymbol{r}_p^i = \boldsymbol{R}_{ti} + \boldsymbol{A}_{ti}\left(\boldsymbol{R}_i^{ti} + \boldsymbol{A}_i^{ti}\boldsymbol{u}_p^i + \boldsymbol{A}_i^{ti}\Phi_p\boldsymbol{q}\right) \tag{2}$$

In Equation (2), Φ_p represents the mode matrix extracted from the modal matrix of the flexible body, which is relevant to the degrees of freedom at point p, and q represents the modal coordinates.

2.2 Algorithm for wheel-rail contact point considering flexible wheelset

For the rigid wheelset, the calculation of the wheel-rail contact point only needs to consider the influence of wheelset motion and the geometric parameters of wheel-rail contact. However, for the flexible wheelset, the influence of wheelset flexibility deformation also needs to be considered. A wheel-rail contact calculation method considered the flexible deformation of the wheelset is established in this paper. Based on the method of the wheel-rail three-dimensional contact geometry based on projection contour for rigid wheelset (Zeng, Wen, Yu, Cheng, & Wang, 2012), the relative position of any point on the wheelset is considered.

Two hypotheses are made in order to get the solution easily:

(1) The stiffness of the wheel tread is relatively high and undergoes minimal deformation. Previous research (Gao, Dai, & Ni, 2012) has found that the outline shape of the wheel rim remains almost unchanged within the frequency range of 5,000Hz for the flexible wheelset. Therefore, it is assumed that wheel tread deformation be neglected, the outer contour shape of the tread remains unchanged.

(2) The deformation of the wheelset is small, which can be represented by modal superposition method.

In addition to the coordinate systems mentioned in section 2.1, four other sets of coordinates are also needed for the wheel-rail contact points calculation, that are the local wheel profile coordinate system $o_w y_w z_w$, local rail profile coordinate system $o_r y_r z_r$, left wheel-rail contact coordinate systems $O'_L X'_L Y'_L Z'_L$ and right wheel-rail contact coordinate systems

$O'_R X'_R Y'_R Z'_R$. The relationships between the trajectory body coordinate system, wheelset body fixed coordinate system, left and right wheel-rail contact coordinate systems, and the local rail profile coordinate system are shown in Figure 2.

As shown in Figure 2, the transformation matrix from the left and right wheel-rail contact coordinate systems to the wheelset body fixed coordinate system can be obtained:

$$\begin{bmatrix} X^i \\ Y^i \\ Z^i \end{bmatrix} = \begin{bmatrix} 1 & 0 & 0 \\ 0 & \cos \delta_{L/R} & \pm \sin \delta_{L/R} \\ 0 & \mp \sin \delta_{L/R} & \cos \delta_{L/R} \end{bmatrix} \begin{bmatrix} x'_{L/R} \\ y'_{L/R} \\ z'_{L/R} \end{bmatrix} \tag{3}$$

In equation (3), δ_L and δ_R represent the left and right wheel rail contact angles respectively. The coordinate transformation from the wheelset body fixed coordinate system to the trajectory body coordinate system is given by:

$$\begin{bmatrix} X^{ti} \\ Y^{ti} \\ Z^{ti} \end{bmatrix} = \begin{bmatrix} \cos \psi & -\sin \psi \cdot \cos \phi & \sin \psi \cdot \sin \phi \\ \sin \psi & \cos \psi \cdot \cos \phi & -\cos \psi \cdot \sin \phi \\ 0 & \sin \phi & \cos \phi \end{bmatrix} \begin{bmatrix} X^i \\ Y^i \\ Z^i \end{bmatrix} \tag{4}$$

In equation (4), ψ and ϕ represent the yaw angle and roll angle of the wheelset, respectively.

For the flexible wheelset, the local wheel profile coordinate system $o_w y_w z_w$, the wheelset body fixed coordinate system, the trajectory body coordinate system and the global coordinate system is shown in Figure 3. Wheelset attitude can be described by the displacements and rotation angles of the wheelset body fixed coordinate system, and the deformation of the wheelset is determined by modal coordinates. For any point P on the wheelset axis, r_p^i denotes its position vector in the wheelset body fixed coordinate system, r_o^i is the position vector of the wheel profile center point o_w in the wheelset body fixed coordinate system. refer to equation (2), the position vector $\boldsymbol{r}_p$ of point P on the wheelset axis in the global coordinate system $OXYZ$ can be expressed as:

$$\boldsymbol{r}_p = \boldsymbol{R}_{ti} + \boldsymbol{A}_{ti} \left(\boldsymbol{r}^w + \boldsymbol{A}_i^{ti} \boldsymbol{r}_p^i + \boldsymbol{A}_i^{ti} \Phi_{wp} \boldsymbol{q}_w \right) \tag{5}$$

In equation (5), $\boldsymbol{r}^w$ represents the position vector of the wheelset body fixed coordinate system in the trajectory body coordinate system; Φ_{wp} is the mode matrix extracted from the wheelset mode matrix related to the degrees of freedom at point P, the extraction of the wheelset mode matrix will be discussed in the next section; $\boldsymbol{q}_w$ represents the modal coordinates of the wheelset.
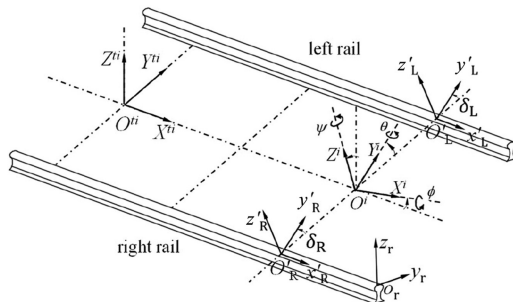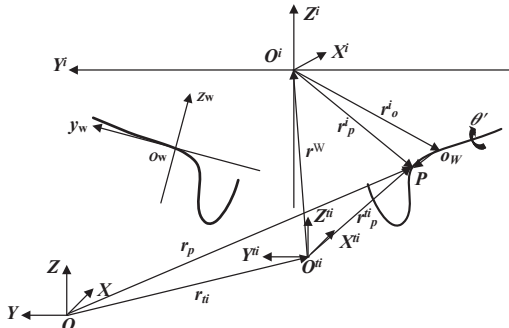

Source(s): Authors' own work

Once the position vector r_p of arbitrarily point on the wheel profile is determined, introducing a variable $\theta' \in [-\pi, \pi]$ named as the roll angle of wheel profile generatrix which is shown in Figure 3. For arbitrary point P on the wheel profile, its coordinates in the wheelset body fixed coordinate system are represented as

$$\left(x_p^i, y_p^i, z_p^i\right) = \left[\left(r_p^i + \Phi_{wp}q_w\right) \cdot i^i, \left(r_p^i + \Phi_{wp}q_w\right) \cdot j^i, \left(r_p^i + \Phi_{wp}q_w\right) \cdot k^i\right]$$

The projection of this point on the $Y^iO^iZ^i$ plane is denoted as $(0, y_p^i, f(y_p^i))$, with $\theta' = 0$ and $f(x)$ represents the fitting function of the wheel profile, it is expressed in the local wheel profile coordinate system $o_w y_w z_w$. Referring to citation (Zeng *et al.*, 2012) sets of spatial coordinates meet the conditions of wheel-rail contact can be expressed on the wheel profile as $(f(y_p^i) \sin \theta', y_p^i, f(y_p^i) \cos \theta')$, where (see Figure 4):

$$\theta' = \arcsin\left(\frac{-f'\left(y_p^i\right)\cos\phi\sin\psi}{\sqrt{(\cos\psi)^2 + (\sin\phi\sin\psi)^2}}\right) - \arctan\left(\frac{\sin\phi\sin\psi}{\cos\psi}\right) \tag{6}$$

In equation (6), ϕ represents the roll angle of the wheel profile and ψ represents the yaw angle of the wheel profile, which includes both the rotation angle of rigid wheelset and the wheel tread yaw and roll angle caused by the elastic deformation of the wheelset, the roll and yaw angle caused by the elastic deformation of wheelset are shown in Figure 5 Assuming that the

Figure 3.
Relationship between the wheel local coordinate system and the global coordinate system

Source(s): Authors' own work
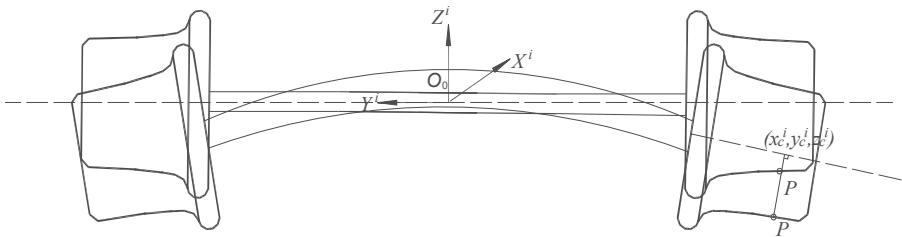
Figure 4.
Solution of possible wheel-rail contact traces considering wheelset deformation

Source(s): Authors' own work

center coordinates of the rolling circle where point P lies are (x_c^i, y_c^i, z_c^i), then the coordinates of the potential wheel-rail contact points in the track coordinate system are represented as:

$$\left(x_p^{ti}, y_p^{ti}, z_p^{ti}\right) = \mathbf{r}^{\mathrm{w}} + A_i^{ti}\left[f\left(y_p^i\right)\sin\theta', y_p^i, f\left(y_p^i\right)\cos\theta' - \mathbf{r}^{\mathrm{w}} + \left(x_c^i, y_c^i, z_c^i\right)\right]^{\mathrm{T}}$$

Based on the method above, the flow chart for the wheel-rail contact points considering wheelset deformation are shown in Figure 6.

3. Railway vehicle model considering flexible wheelset

3.1 Creating wheelset finite element model and the selection of modal

The wheelset finite element model is established in software ABAQUS as shown in Figure 7, the wheel profile is S1002 and the wheelset axle is designed as a lightweight hollow axle. The minimum mesh size is set to 2 mm, the model has 110,592 elements and 135,217 nodes.

The wheelset modal information shown in Table 1 is selected to establish the wheelset flexible model. 1 - 8th order modes are selected, excluding rigid body modes. These modes mainly involve the deformation modes of the wheelset axle and wheel web, the frequency range is within 500 Hz.
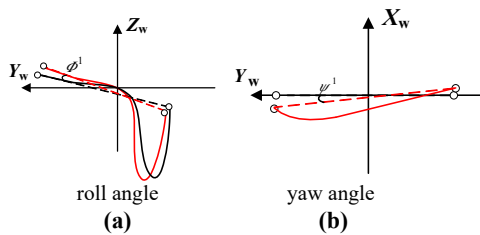
Figure 5.
Roll and yaw angle caused by the elastic deformation of wheelset

roll angle
(a)

yaw angle
(b)
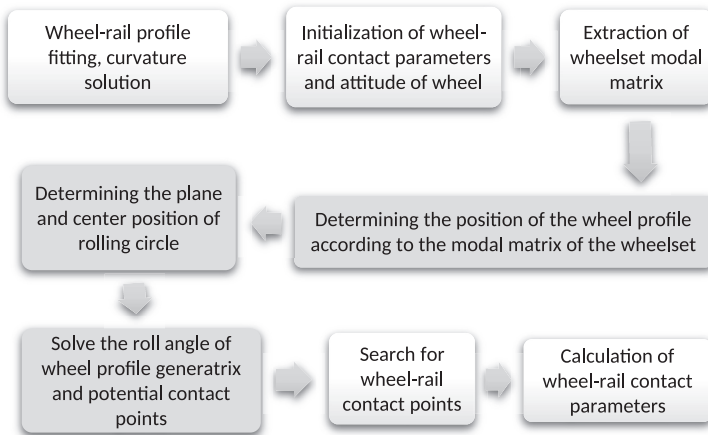
Source(s): Authors' own work

Figure 6.
Implementation process of flexible wheel rail geometry contact problem

Source(s): Authors' own work

3.2 Approach for establishing vehicle dynamics equations considering wheelset flexibility
This section introduces the establishment of a flexible wheelset model that considers the influence of wheel rotation, based on the Lagrangian method, nonlinear differential-algebraic equations for vehicle multibody system can be established (Hussein & Shabana, 2011), as shown in Equation (5).

$$\begin{cases} \boldsymbol{M}(\boldsymbol{q})\ddot{\boldsymbol{q}} + \Phi_q^{\mathrm{T}}\lambda = \boldsymbol{Q}\left(\dot{\boldsymbol{q}}, \boldsymbol{q}, t\right) \\ \boldsymbol{C}(\boldsymbol{q}, t) = \boldsymbol{0} \end{cases} \tag{5}$$

In Equation (5), $\boldsymbol{M}$ represents the generalized mass matrix of the vehicle system; q denotes the generalized coordinate vector of the vehicle system, $\boldsymbol{q} = [q_1, q_2, \cdots q_k]^{\mathrm{T}}$, Φ_q stands for the constraint Jacobian matrix of the vehicle system, λ is the Lagrange multiplier matrix, $\boldsymbol{Q}$ represents the generalized force matrix, including external and internal forces, and $\boldsymbol{C}(\boldsymbol{q}, t) = \boldsymbol{0}$ represents the constraint equations of the vehicle system.

The forces acting on vehicle components mainly include the wheel-rail contact forces/moments and the forces/moments provided by the vehicle suspension system. The contribution of the primary and secondary suspension elements to the generalized force vector of the vehicle system is included in the generalized force matrix $\boldsymbol{Q}$, and wheel-rail contact forces are treated as a special kind of force element.

For flexible vehicle system, the generalized external force expression can be derived based on the virtual work principle. The forces from the force elements are applied to the Maker point fixed on the body. The components of the external force and external torque in the global coordinate system are denoted as $\boldsymbol{F}_{Glo}$ and $\boldsymbol{M}_{Glo}$ respectively, the virtual work of external forces is expressed as:

$$\delta \boldsymbol{W}^e = \delta \boldsymbol{r}_I^{\mathrm{T}} \boldsymbol{F}_{Glo} + \delta \varphi_I^{\mathrm{T}} \boldsymbol{M}_{Glo} = \delta \boldsymbol{\xi}^{\mathrm{T}} \left(\left(\frac{d\boldsymbol{r}_I}{d\boldsymbol{\xi}}\right)^{\mathrm{T}} \boldsymbol{F}_{Glo} + \left(\frac{d\varphi_I}{d\boldsymbol{\xi}}\right)^{\mathrm{T}} \boldsymbol{M}_{Glo} \right) = \delta \boldsymbol{\xi}^{\mathrm{T}} \boldsymbol{Q}^e \tag{6}$$

In Equation (6), $\boldsymbol{r}_I$ and φ_I respectively represents the global position vector and the rotation vector of the Maker point fixed to the body. $\delta \boldsymbol{r}_I$ and $\delta \varphi_I$ represent virtual displacements and virtual rotation angular respectively, and $\delta \boldsymbol{\xi}$ represents the isochronous variation of generalized coordinates. According to Equation (6), the generalized external force relative to the trajectory body coordinate system is:

$$\boldsymbol{Q}^e = \left(\frac{d\boldsymbol{r}_I}{d\boldsymbol{\xi}}\right)^{\mathrm{T}} \boldsymbol{F}_{Glo} + \left(\frac{d\varphi_I}{d\boldsymbol{\xi}}\right)^{\mathrm{T}} \boldsymbol{M}_{Glo} \tag{7}$$

The generalized force transformation matrix can be derived which is shown as following.
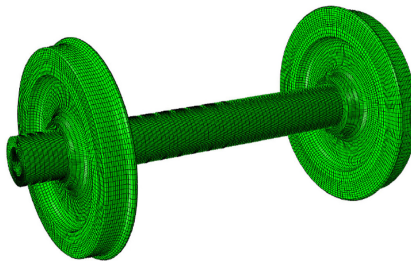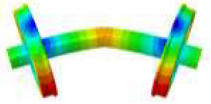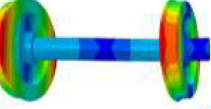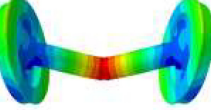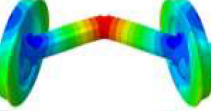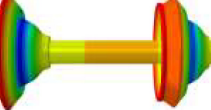
Source(s): Authors' own work

Mode Number	Frequency/Hz	Mode Description	Mode Shape Diagram
1	92.024	first order vertical bending mode	
2	92.024	first order longitudinal bending mode	
3	184.85	second order vertical bending mode	
4	184.85	second order longitudinal bending mode	
5	273.69	first order umbrella shape mode	
6	324.53	third order vertical bending mode	
7	324.53	third order longitudinal bending mode	
8	474.72	second order umbrella shape mode	

Source(s): Authors' own work

Table 1.
Modal information of
the wheelset

$$\delta \boldsymbol{r}_I = \delta \boldsymbol{R}_{ti} + \delta \boldsymbol{A}_{ti}\left(\overline{\boldsymbol{R}}^i + \boldsymbol{A}_i^{ti}\overline{\boldsymbol{\rho}}_I^i + \boldsymbol{A}_i^{ti}\Phi_I \boldsymbol{q}\right) + \boldsymbol{A}_{ti}\left(\delta\overline{\boldsymbol{R}}^i + \delta \boldsymbol{A}_i^{ti}\left(\overline{\boldsymbol{\rho}}_I^i + \Phi_I \boldsymbol{q}\right) + \boldsymbol{A}_i^{ti}\Phi_I \delta \boldsymbol{q}\right)$$

$$= \left[\boldsymbol{i}_{ti} + \frac{\partial \boldsymbol{A}_{ti}}{\partial s^i}\left(\overline{\boldsymbol{R}}^i + \boldsymbol{A}_i^{ti}\overline{\boldsymbol{\rho}}_I^i + \boldsymbol{A}_i^{ti}\Phi_I \boldsymbol{q}\right) \quad \boldsymbol{j}_{ti} \quad \boldsymbol{k}_{ti} \quad -\boldsymbol{A}_{ti}\boldsymbol{A}_i^{ti}\left(\widetilde{\overline{\boldsymbol{\rho}}}_I^i + q_m\widetilde{\Phi}_{Im}\right)\overline{\boldsymbol{G}}^i \boldsymbol{A}_{ti}\boldsymbol{A}_i^{ti}\Phi_I\right]\dot{\boldsymbol{\xi}} \tag{8}$$

In Equation (8), $\boldsymbol{i}_{ti}$, $\boldsymbol{j}_{ti}$, and $\boldsymbol{k}_{ti}$ are column vectors of the coordinate transformation matrix $\boldsymbol{A}_{ti}$, $\tilde{\boldsymbol{a}}$ represents the skew-symmetric matrix of vector $\boldsymbol{a}$, Φ_I is the extracted wheelset modal matrix, $\boldsymbol{G}^i$ and $\overline{\boldsymbol{G}}^i$ are the transformation matrices about Euler angles $\boldsymbol{\theta}^i$.

$$\boldsymbol{G}^i = \boldsymbol{A}^i \overline{\boldsymbol{G}}^i = \begin{bmatrix} 0 & \cos\psi^i & -\sin\psi^i\cos\varphi^i \\ 0 & \sin\psi^i & \cos\psi^i\cos\varphi^i \\ 1 & 0 & \sin\varphi^i \end{bmatrix} \tag{9}$$

$$\overline{\boldsymbol{G}}^i = \boldsymbol{A}^{i\mathrm{T}}\boldsymbol{G}^i = \begin{bmatrix} -\cos\varphi^i\sin\theta^i & \cos\theta^i & 0 \\ \sin\varphi^i & 0 & 1 \\ \cos\varphi^i\cos\theta^i & \sin\theta^i & 0 \end{bmatrix} \tag{10}$$

For the rigid body, Equation (8) can be simplified as:

$$\delta\boldsymbol{r}_I = \delta\boldsymbol{R}_{ti} + \delta\boldsymbol{A}_{ti}\left(\overline{\boldsymbol{R}}^i + \boldsymbol{A}^{ti}_i\overline{\boldsymbol{\rho}}^i_I\right) + \boldsymbol{A}_{ti}\left(\delta\overline{\boldsymbol{R}}^i + \delta\boldsymbol{A}^{ti}_i\overline{\boldsymbol{\rho}}^i_I\right)$$
$$= \left[\boldsymbol{i}_{ti} + \frac{\partial\boldsymbol{A}_{ti}}{\partial s^i}\left(\overline{\boldsymbol{R}}^i + \boldsymbol{A}^{ti}_i\overline{\boldsymbol{\rho}}^i_I\right) \quad \boldsymbol{j}_{ti} \quad \boldsymbol{k}_{ti} \quad -\boldsymbol{A}_{ti}\boldsymbol{A}^{ti}_i\tilde{\overline{\boldsymbol{\rho}}}^i_I\overline{\boldsymbol{G}}^i \right]\dot{\boldsymbol{\xi}} \tag{11}$$

Similarly, the generalized torque transformation matrix $d\varphi^i/d\boldsymbol{\xi}$ can be derived based on Equation (12).

$$\delta\boldsymbol{\varphi}^I = \boldsymbol{G}^{ti}\frac{d\boldsymbol{\theta}^{ti}}{ds}\delta s + \boldsymbol{A}^{ti}\boldsymbol{A}^i\left(\overline{\boldsymbol{G}}^i\delta\boldsymbol{\theta}^i + \boldsymbol{\psi}^i\delta\boldsymbol{q}^i\right)$$
$$= \left[\boldsymbol{G}^{ti}\frac{d\boldsymbol{\theta}^{ti}}{ds} \quad 0 \quad 0 \quad \boldsymbol{A}^{ti}\boldsymbol{A}^i\overline{\boldsymbol{G}}^i \quad \boldsymbol{A}^{ti}\boldsymbol{A}^i\boldsymbol{\psi}^i \right]\delta\boldsymbol{\xi} \equiv \frac{d\boldsymbol{\varphi}^I}{d\boldsymbol{\xi}}\delta\boldsymbol{\xi} \tag{12}$$

In Equation (12), $\boldsymbol{\psi}^i$ represents the rotational modal matrix at point P, for the rigid body, Equation (12) can be simplified as:

$$\delta\boldsymbol{\varphi}^I = \boldsymbol{G}^{ti}\frac{d\boldsymbol{\theta}^{ti}}{ds}\delta s + \boldsymbol{A}^{ti}\boldsymbol{A}^i\left(\overline{\boldsymbol{G}}^i\delta\boldsymbol{\theta}^i\right) = \left[\boldsymbol{G}^{ti}\frac{d\boldsymbol{\theta}^{ti}}{ds} \quad 0 \quad 0 \quad \boldsymbol{A}^{ti}\boldsymbol{A}^i\overline{\boldsymbol{G}}^i \right]\delta\boldsymbol{\xi} \equiv \frac{d\boldsymbol{\varphi}^I}{d\boldsymbol{\xi}}\delta\boldsymbol{\xi} \tag{13}$$

The kinetic energy of the flexible wheelset can be expressed as:

$$T^i = \frac{1}{2}\iiint \rho^i\dot{\boldsymbol{r}}^{j\,\mathrm{T}}_p\dot{\boldsymbol{r}}^j_p dV = \frac{1}{2}\dot{\boldsymbol{\xi}}^{i\,\mathrm{T}}\left(\iiint \boldsymbol{L}^{\mathrm{T}}\boldsymbol{L}dm^i_p\right)\dot{\boldsymbol{\xi}}^i = \frac{1}{2}\dot{\boldsymbol{\xi}}^{i\,\mathrm{T}}\boldsymbol{M}^i\dot{\boldsymbol{\xi}}^i \tag{14}$$

Therefore, the first kind of Lagrangian equation is

$$\frac{d}{dt}\frac{\partial T}{\partial\dot{\boldsymbol{\xi}}^i} - \frac{\partial T}{\partial\boldsymbol{\xi}^i} = \boldsymbol{Q}^a + \boldsymbol{Q}^v \tag{15}$$

The generalized acceleration terms in the inertial force in Equation (15) is:

$$\boldsymbol{Q}^a = \int_V \boldsymbol{L}^{\mathrm{T}}\boldsymbol{L}\ddot{\boldsymbol{\xi}}dm = \boldsymbol{M}^i\ddot{\boldsymbol{\xi}}^i \tag{16}$$

The block form of the mass matrix $\boldsymbol{M}^i$ is given by:

$$\boldsymbol{M}^i = \begin{bmatrix} M_{11} & M_{12} & M_{13} & \boldsymbol{M}_{14} & \boldsymbol{M}_{15} \\ & M_{22} & M_{23} & \boldsymbol{M}_{24} & \boldsymbol{M}_{25} \\ & & M_{33} & \boldsymbol{M}_{34} & \boldsymbol{M}_{35} \\ & & & \boldsymbol{M}_{44} & \boldsymbol{M}_{45} \\ sym & & & & \boldsymbol{M}_{55} \end{bmatrix} \tag{17}$$

The quadratic generalized speed term in the inertial force is given by:

$$\boldsymbol{Q}^v = \int\limits_V \boldsymbol{L}^{\mathrm{T}} \dot{\boldsymbol{L}} \dot{\boldsymbol{\xi}} dm \tag{18}$$

For the rigid wheelset, the wheel-rail force can be directly applied to the wheelset's center of mass as resultant force and moment, then these forces can be transformed into generalized forces corresponding to the six generalized coordinates of the wheelset. $\boldsymbol{F}_{Glo}$ and $\boldsymbol{M}_{Glo}$ in Equation (7) can be calculated as follows:

$$\begin{aligned} \boldsymbol{F}_{Glo} &= \boldsymbol{F}_{\mathrm{R}} + \boldsymbol{F}_{\mathrm{L}} \\ \boldsymbol{M}_{Glo} &= \widetilde{\boldsymbol{L}}_{\mathrm{R}} \boldsymbol{F}_{\mathrm{R}} + \widetilde{\boldsymbol{L}}_{\mathrm{L}}^{\mathrm{T}} \boldsymbol{F}_{\mathrm{L}} \end{aligned} \tag{19}$$

In equation (19), $\boldsymbol{F}_{\mathrm{L}}$ represents the left wheel-rail contact force, $\boldsymbol{F}_{\mathrm{R}}$ represents the right wheel-rail contact force, $\boldsymbol{L}_{\mathrm{L}} = \{L_{XL}, L_{YL}, L_{ZL}\}$ represents the position vector from the left wheel-rail contact point to the wheelset center, and $\boldsymbol{L}_{\mathrm{R}} = \{L_{XR}, L_{YR}, L_{ZR}\}$ represents the position vector from the right wheel-rail contact point to the wheelset center.

The forces of the wheelset is shown in Figure 8, where the generalized coordinates of the wheelset are denoted by $\boldsymbol{q}_{\mathrm{w}} = [\boldsymbol{q}_{\mathrm{wG}}^{\mathrm{T}}, \boldsymbol{q}_{\mathrm{wf}}^{\mathrm{T}}]^{\mathrm{T}} \in \boldsymbol{R}^n$, with the six rigid body degrees of freedom denoted as $\boldsymbol{q}_{\mathrm{wG}}^{\mathrm{T}} = [x, y, z, \phi, \theta, \psi]^{\mathrm{T}}$. Figure 8 only illustrates the forces acted on the wheelset in the single contact point case, the situation with multiple contact points is similar. The wheel-rail contact forces shown in Figure 8 are descried in Table 2, all forces are defined in the wheelset body fixed coordinate system. The wheel-rail contact forces in equation (14) can be represented by the forces in Table 2:

$$\begin{aligned} \boldsymbol{F}_{\mathrm{L}} &= \{ F_{xli} + N_{xli}, F_{yli} + N_{yli}, F_{zli} + N_{zli} \}^{\mathrm{T}} \\ \boldsymbol{F}_{\mathrm{R}} &= \{ F_{xri} + N_{xri}, F_{yri} + N_{yri}, F_{zri} + N_{zri} \}^{\mathrm{T}} \end{aligned} \tag{20}$$

Using the coordinate transformation matrix, the distance from the contact point to the center of the wheelset is converted into the coordinates of the trajectory body system, as shown in Equation (21) and Figure 9.
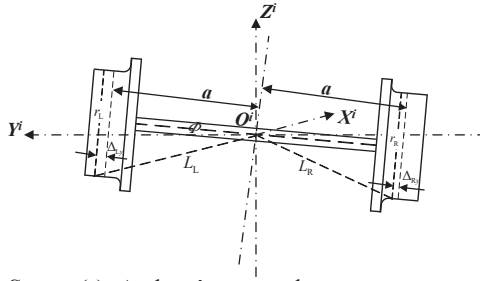

Source(s): Authors' own work

Symbol	Meaning	Symbol	Meaning
F_{xli},F_{xri}	longitudinal component of left/right wheel rail creep force of ith wheelset	F_{yli},F_{yri}	lateral component of left/right wheel rail creep force of ith wheelset
F_{zli},F_{zri}	vertical component of left/right wheel rail creep force of ith wheelset	N_{xli},N_{xri}	longitudinal component of left/right wheel rail creep force of ith wheelset
N_{yli},N_{yri}	lateral component of left/right wheel rail normal force of ith wheelset	N_{zli},N_{zri}	vertical component of left/right wheel rail creep force of ith wheelset
M_{xli},M_{xri}	longitudinal component of left/right wheel rail creep moment of ith wheelset	M_{yli},M_{yri}	lateral component of left/right wheel rail creep moment of ith wheelset
M_{zli},M_{zri}	vertical component of left/right wheel rail creep moment of ith wheelset		

Note(s): Wheelset body fixed coordinate
Source(s): Authors' own work

Table 2.
The parameters
description of wheel
rail contact force

Figure 9.
Distance from the
contact point to the
center of the wheelset

Source(s): Authors' own work

$$L_{XL/R} = (a \mp \Delta_{L/Ry})\sin\psi\cos\phi \pm r_{L/R}\sin\psi\sin\phi$$
$$L_{YL/R} = (a \mp \Delta_{L/Ry})\cos\phi\cos\psi \pm r_{L/R}\cos\psi\sin\phi \quad (21)$$
$$L_{ZL/R} = r_{L/R}\cos\phi \mp (a \mp \Delta_{L/Ry})\sin\phi$$

In Equation (21), a represents the distance from the center of wheel nominal rolling circle to the center of the wheelset, r_L and r_R respectively represent the radii of the left and right wheel-rail contact rolling circles, Δ_{Lx} and Δ_{Rx} respectively represent the longitudinal displacement of the left and right wheel-rail contact points from their original positions in the wheelset body fixed coordinate system. Δ_{Ly} and Δ_{Ry} respectively represent the lateral displacement of the left and right wheel-rail contact points from their original positions, all of the above geometry parameter can be solved by the three-dimensional geometric contact calculation.

As for the flexible wheelset, generalized force in modal coordinates generated by the elastic deformation of the wheelset also make contribution to the wheel-rail contact force, and it can't be simply applied to the wheel rail contact point, more work is required. In this paper, the wheel-rail contact forces are applied to four grid nodes near the contact point.

The equivalent method for the wheel-rail flexible contact forces is illustrated in Figure 10. Firstly, it's necessary to discretize the wheelset profile into rotationally symmetric grids, for the contact point P shown in Figure 10, four nodes P_1 - P_4 near the contact point can be found, then the generalized force weighted values of the four nodes can be obtained by the angular values of adjacent nodes.

The generalized wheel-rail contact force is equivalent to the weighted sum of the generalized forces calculated at these four nodes, that is:

$$\boldsymbol{Q}_c^e = \sum \alpha_i \boldsymbol{Q}_{ci}^e, i = 1, 2, 3, 4 \tag{22}$$

In equation (22), $\boldsymbol{Q}_{ci}^e$ represents the generalized force equivalent to the contact force at node P_i, and α_i represents the weighting coefficient, expressed as:

$$\alpha_1 = \frac{y_{P23} - y_P}{y_{P23} - y_{P41}} \frac{\theta_{P4} - \theta_{P41}}{\theta_{P4} - \theta_{P1}}, \alpha_2 = \frac{y_{P23} - y_P}{y_{P23} - y_{P41}} \frac{\theta_{P41} - \theta_{P1}}{\theta_{P4} - \theta_{P1}}$$

$$\alpha_3 = \frac{y_P - y_{P41}}{y_{P23} - y_{P41}} \frac{\theta_{P3} - \theta_{P23}}{\theta_{P3} - \theta_{P2}}, \alpha_4 = \frac{y_P - y_{P41}}{y_{P23} - y_{P41}} \frac{\theta_{P23} - \theta_{P2}}{\theta_{P3} - \theta_{P2}} \tag{23}$$

Once the wheel-rail contact force is obtained, the generalized external force relative to the track coordinate can be obtained when substituting it into equation (7).

3.3 Calculation of the Jacobian matrix for the wheel-rail contact force

According to the general form of the vehicle multibody dynamics equation introduced in the previous section (Equation 5), let $\boldsymbol{y} = \left(\boldsymbol{q}^T, \quad \boldsymbol{\lambda}^T\right)^T$ and $\boldsymbol{\lambda} = (\lambda_1, \cdots, \lambda_m)^T$, the equation can be written in a more general form as:

$$\boldsymbol{F}\left(\boldsymbol{y}, \dot{\boldsymbol{y}}, \ddot{\boldsymbol{y}}, t\right) = \boldsymbol{0} \tag{24}$$

The symbols $\dot{\boldsymbol{y}}$ and $\ddot{\boldsymbol{y}}$ in the equation represent first and second order derivatives of $\boldsymbol{y}$ with respect to time. Equation (19) is solved by implicit integration methods, the differential-algebraic equation is transformed into the nonlinear equation with the unknown variables at the current time, a Jacobian matrix is required to solve this nonlinear equation.

In Equation (5), the generalized force of the wheel-rail contact force is denoted as $\boldsymbol{Q}_w \in \boldsymbol{R}^n$, when the Newton iteration numerical method is used to solve the equation, the term in right-hand side of the equation generated by the wheel-rail contact force is $-\boldsymbol{Q}_w$, the contribution of the Jacobian matrix is:

$$\boldsymbol{A} = \left(\alpha^2 \partial \boldsymbol{Q}_w / \partial \ddot{\boldsymbol{q}}_w + \alpha \partial \boldsymbol{Q}_w / \partial \dot{\boldsymbol{q}}_w + \partial \boldsymbol{Q}_w / \partial \boldsymbol{q}_w\right) \tag{25}$$

In Equation (25), $\alpha = 1/\Delta t$, Δt represents the current integration step, defined as $\Delta t = t_{n+1} - t_n$. Since these expressions $\partial \boldsymbol{Q}_w / \partial \boldsymbol{q}_w$, $\partial \boldsymbol{Q}_w / \partial \dot{\boldsymbol{q}}_w$ and $\partial \boldsymbol{Q}_w / \partial \ddot{\boldsymbol{q}}_w$ cannot be expressed in analytical form, special methods are required. In this paper, the numerical
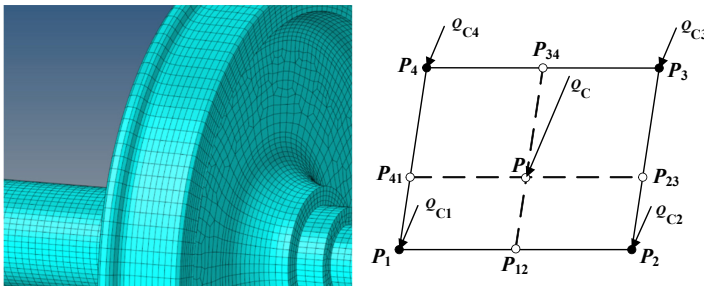
Source(s): Authors' own work

difference method (Kan, Peng, & Chen, 2017) was used to compute the Jacobian matrix of the wheel-rail contact force, that is give each generalized coordinate $\boldsymbol{q}_{\mathrm{w}}$ a perturbation by Δq_i, solve the variation of the wheel-rail contact generalized force caused by this perturbation, and then divide it by the perturbation value to obtain the corresponding Jacobian matrix.

The partitioned matrices of Jacobian matrix is $\boldsymbol{A} = [\,\boldsymbol{A}_1 \quad \cdots \quad \boldsymbol{A}_n\,]$ and $\boldsymbol{A}_i$ can be calculated using the following expression:

$$A_i = \frac{Q_{\mathrm{w}}\left(\boldsymbol{q}_{\mathrm{w}} + \Delta q_i \boldsymbol{e}_i, \dot{\boldsymbol{q}}_{\mathrm{w}} + \alpha \Delta q_i \boldsymbol{e}_i, \ddot{\boldsymbol{q}}_{\mathrm{w}} + \alpha^2 \Delta q_i \boldsymbol{e}_i\right) - Q_{\mathrm{w}}\left(\boldsymbol{q}_{\mathrm{w}}, \dot{\boldsymbol{q}}_{\mathrm{w}}, \ddot{\boldsymbol{q}}_{\mathrm{w}}\right)}{\Delta q_i} \tag{26}$$

Since the wheel-rail forces are independent of the generalized coordinate accelerations, the acceleration terms above can be ignored, that is:

$$A_i = \frac{Q_{\mathrm{w}}\left(\boldsymbol{q}_{\mathrm{w}} + \Delta q_i \boldsymbol{e}_i, \dot{\boldsymbol{q}}_{\mathrm{w}} + \alpha \Delta q_i \boldsymbol{e}_i\right) - Q_{\mathrm{w}}\left(\boldsymbol{q}_{\mathrm{w}}, \dot{\boldsymbol{q}}_{\mathrm{w}}\right)}{\Delta q_i} \tag{27}$$

including $\boldsymbol{e}_i = \begin{bmatrix} 0 & \cdots & 1 & 0 \\ 1 & & i & 6 \end{bmatrix}$.

4. Discussion on dynamic response of flexible wheelset
A vehicle dynamics model is established as an example, the wheelsets are considered both as rigid and flexible body, two kinds of track excitations are used, that are the measured track irregularity and periodic short-wave irregularities. The analyses cases are described in Table 3.

The excitation frequency caused by short-wave irregularities can be calculated by $f = v/(3.6l)$, and Table 4 shows the short-wave excitation frequencies change with vehicle speed.

The simulation results of vertical wheel-rail force in the time-domain of the rigid and flexible wheelset models as for Case1-1 to Case1-6 are shown in Figure 11, it can be seen that under measured track irregularity, the amplitude of the vertical wheel-rail force simulated by the flexible wheelset model is smaller than that of the rigid wheelset model. Additionally, as the increases of speed, the discrepancy of the vertical force amplitude obtained by the flexible and rigid wheelset models become more obvious, when the speed increases to 400 km/h from

Case	Running speed /(km/h)	Lateral irregularity	Vertical irregularity
1-1	200	Measured track irregularities	Measured track irregularities
1-2	250		
1-3	300		
1-4	330		
1-5	350		
1-6	400		
2-1	200	–	A sine wave with a wavelength of 0.4 m and an amplitude of 0.04 mm
2-2	250		
2-3	280		
2-4	350		

Source(s): Authors' own work

Table 3.
Analyses cases

200 km/h, the peak value of the vertical wheel-rail force calculated by the rigid wheelset model is doubled compared to the flexible wheelset.

The longitudinal and lateral wheel-rail forces calculated by the rigid wheelset and flexible wheelset models are illustrated in Figures 12 and 13 in Case1-2, Case1-5 and Case1-6. For the Case1-2 when the speed is 250 km/h, the amplitude difference is small for both the longitudinal and lateral wheel-rail forces calculated by the rigid and flexible wheelset model, as the speed increases to 400 km/h, the longitudinal and lateral wheel-rail forces calculated by the rigid wheelset model become significantly larger than those of the flexible wheelset model, furthermore, the wheel-rail forces of rigid wheelset model exhibits fluctuations and large peak values, indicating that the rigid wheelset model is more sensitive to the impact of track compared to the flexible wheelset model. It can be seen that as the speed increases, the discrepancies in wheel-rail longitudinal and lateral forces calculated by the flexible and rigid wheelset models become larger. For the case of speeds equal to 350 km/h and above, it is necessary to choose an appropriate model to get simulation results which will agree better with the reality.

Taking Case1-3 as an example, a comparison results of the wheel-rail equivalent contact patch and virtual penetration are shown in Figure 14 obtained by the two models, it can be observed that at a speed of 300 km/h, the virtual penetration and equivalent contact area calculated by the rigid wheelset model are larger than those of the elastic model. The

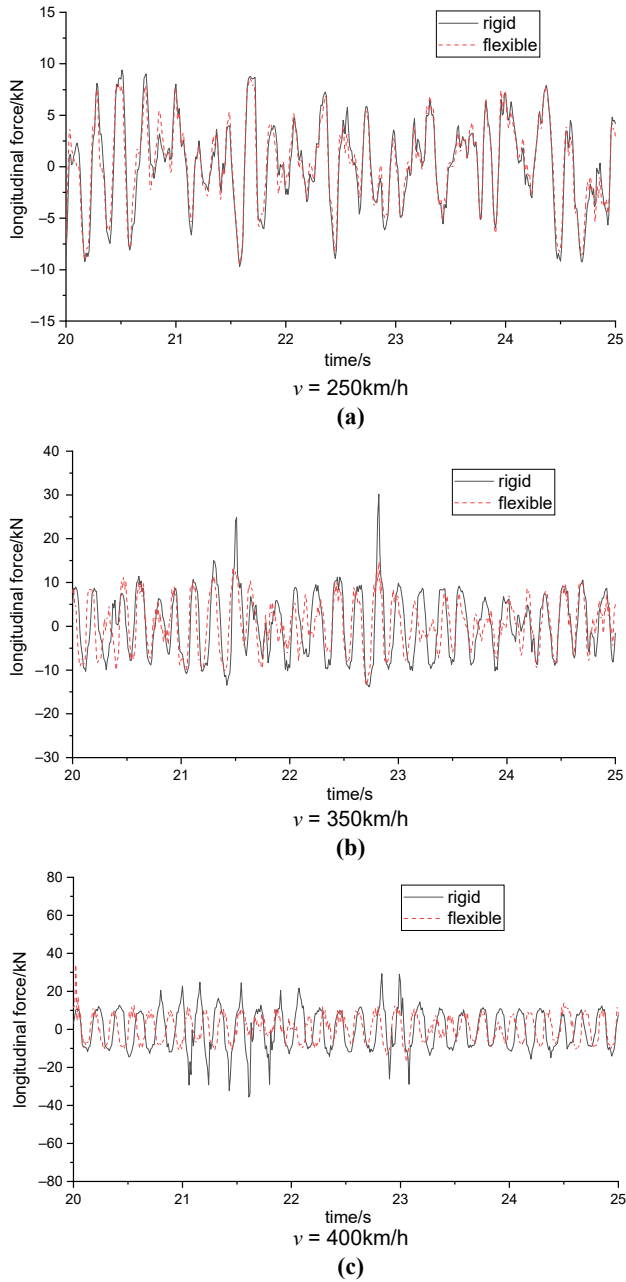| Running speed/(km/h)	200	250	280	350
impact frequency/Hz	138.89	173.61	194.44	243.05
Source(s): Authors' own work				

Table 4.
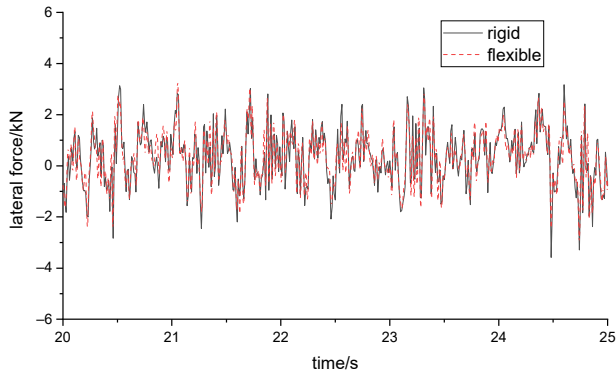Impact frequency vs running speed
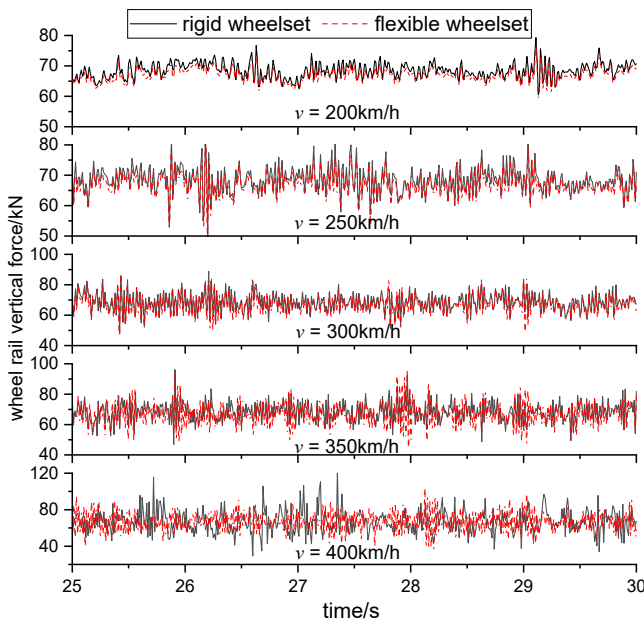
Figure 11.
Wheel rail vertical force

Source(s): Authors' own work

Figure 12.
Comparative results of
wheel rail
longitudinal force

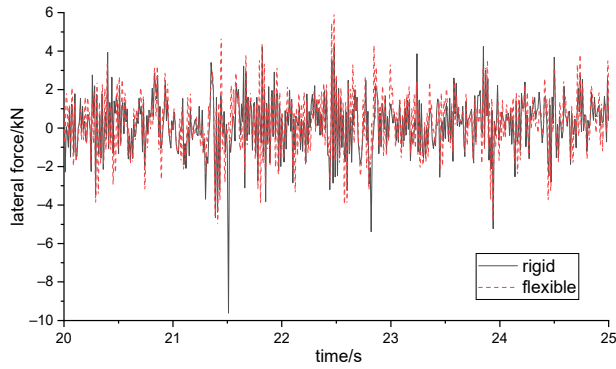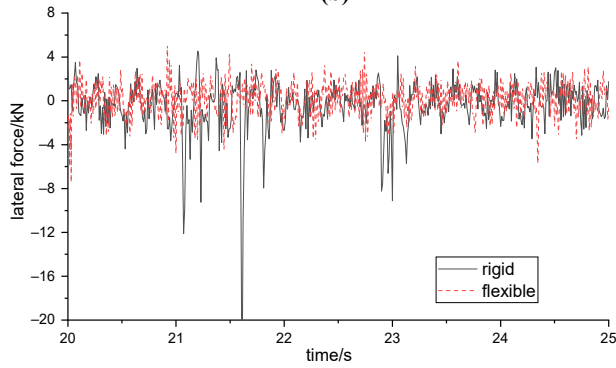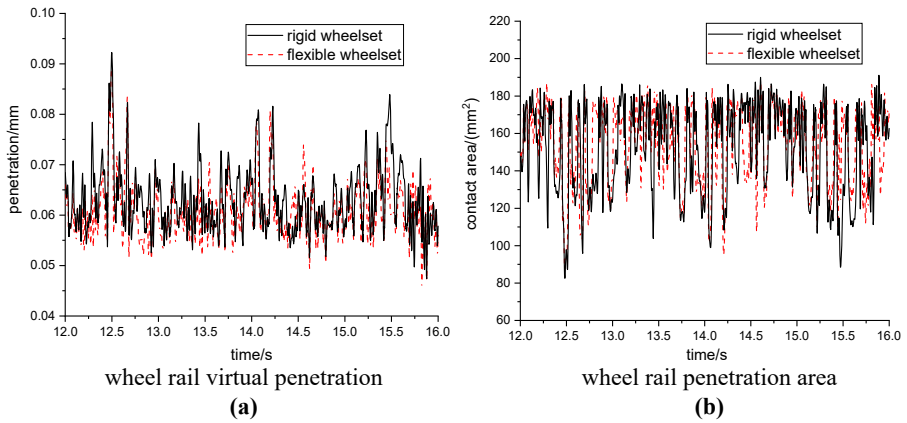**Source(s):** Authors' own work

$v = 250$km/h

(a)

$v = 350$km/h

(b)

$v = 400$km/h

(c)

Source(s): Authors' own work

Source(s): Authors' own work

fluctuations of wheel-rail geometric contact results are more obvious for the rigid wheelset model, at 15.5 seconds, there is a sudden increase in wheel-rail penetration for the rigid contact model, leading to a sudden change in the wheel-rail contact area. The flexible model, by considering the elastic deformation of the wheelset during the contact point solution, can better reflect the actual wheel-rail contact state.

The wheel-rail creepage obtained by the two models in Case 1–3 (300 km/h) are shown in Figure 15. When considering the elastic deformation of the wheelset, the longitudinal and lateral creepages are slightly reduced than that of rigid wheelset model. In addition to being influenced by the geometric contact parameters, the structural vibration of the flexible wheelset will also generate additional velocity at the wheel-rail contact points apart from the rigid wheelset velocity. These contribute to the differences in creepage calculated by the flexible and rigid wheelset models.

As for the Case 2-1 to Case 2-4, the time-domain comparison results of wheel rail vertical force are illustrated in Figure 16, it can be observed that under short-wave excitation, the amplitude of the vertical wheel-rail force calculated by the flexible wheelset is also smaller
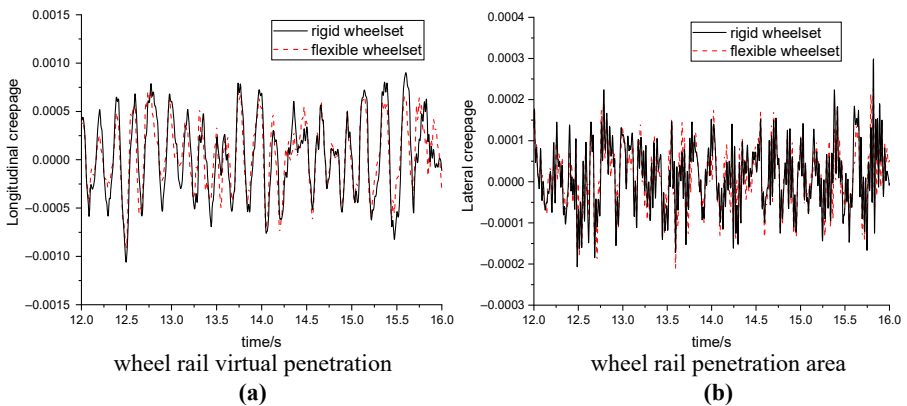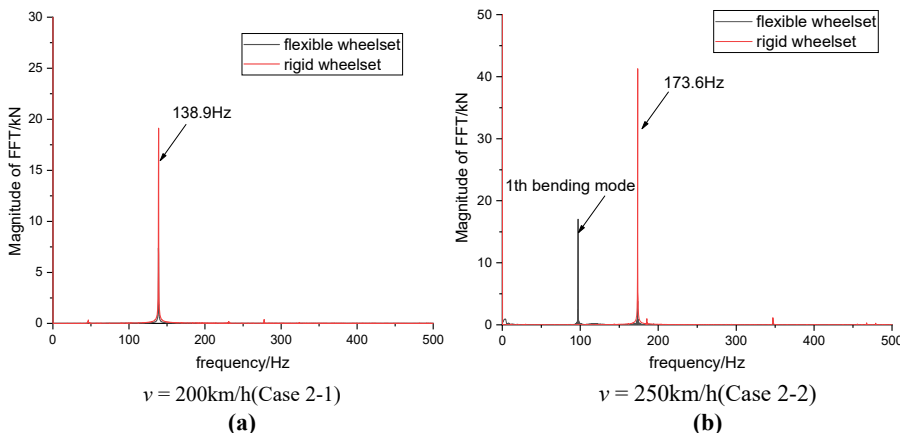
Source(s): Authors' own work

than that of the rigid wheelset. The comparison results of frequency characteristics for vertical force are shown in Figure 17, which reveal that at a speed of 200 km/h, both rigid and flexible wheelsets exhibit high-frequency vibrations at the short-wave excitation frequency of 138.89 Hz. When the speed increases to 250 km/h, the flexible wheelset not only undergoes forced vibration at a frequency of 173.6 Hz under short-wave excitation but also at a frequency of 92 Hz which is equal to the first-order vertical bending vibration mode frequency. What should be noted is that, unlike the excitation case of measured track irregularities, under short-wave excitation, as the speed change from 200 to 350 km/h, the amplitude discrepancy of the vertical force calculated by two models gradually decrease with the speed, due partly to the vibration elastic modes is produced by the short-wave excitation which will occur in some operating conditions.

Fleaxible wheelset model
(a)

Rigid wheelset model
(b)

Source(s): Authors' own work
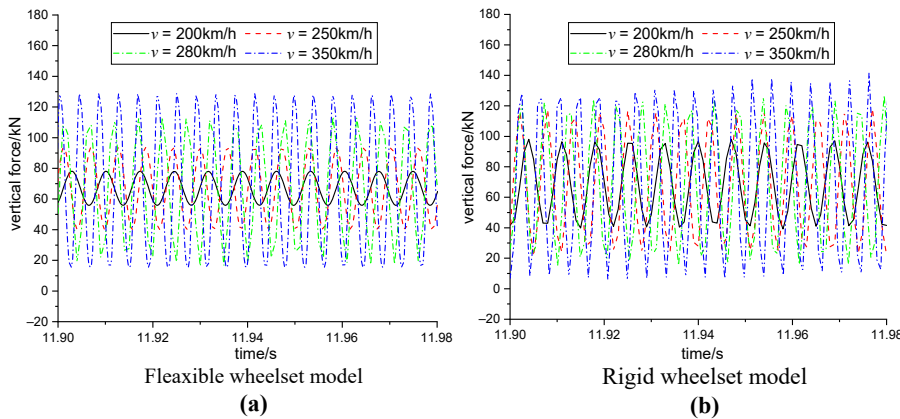
Figure 16.
Comparative results of wheel rail vertical force

v = 200km/h(Case 2-1)
(a)

v = 250km/h(Case 2-2)
(b)

Source(s): Authors' own work

Figure 17.
Frequency characteristics of wheel rail vertical force

5. Conclusion

(1) The comparative analysis of the rigid and flexible wheelset models under measured track irregularities reveals that: the amplitudes of vertical, longitudinal and lateral wheel-rail forces computed by the flexible wheelset model are all smaller than those by the rigid wheelset model. The rigid wheelset model is more sensitive to the impacts from track irregularities compared to the flexible wheelset model. Moreover, as the vehicle speed increases, the amplitude differences of wheel-rail forces computed by the flexible and rigid wheelset models become larger.

(2) Under normal track irregularities, the rigid wheelset model gives larger virtual penetration and equivalent contact areas results compared to the elastic wheelset model. Additionally, the fluctuations of wheel-rail geometric contact results are more obvious for the rigid wheelset model, there is a slight decrease in both longitudinal and lateral creepages for the flexible wheelset model, thus for low-frequency wheel-rail force analysis problems at speeds of 350 km/h and above, the flexible wheelset model is recommended and will give results agrees better with the reality.

(3) Under short-wave track excitation, the flexible wheelset model also gives smaller results of vertical wheel-rail forces compared to the rigid wheelset. However, unlike the excitation case of measured track irregularity, under short-wave excitations, for the speed within the range of 200 to 350 km/h, the difference in the amplitude of the vertical force between the flexible and rigid wheelset models gradually decreases as the speed increase. This is partially due to the excitation of elastic vibration modes of the wheelset under short-wave irregularities.

References

Baeza, L., Fayos, J., Roda, A., & Insa, R. (2008). High frequency railway vehicle-track dynamics through flexible rotating wheelsets. *Vehicle System Dynamics*, *46*(7), 647–659. doi: 10.1080/00423110701656148.

Casanueva, C., Alonso, A., Eziolaza, I., & Jose, G. (2014). Simple flexible wheelset model for low-frequency instability simulations. *Proceedings of the Institution of Mechanical Engineers, Part F. Journal of Rail and Rapid Transit*, *228*(2), 169–181. doi: 10.1177/0954409712468253.

Cui, X., Yao, J., Hu, X., Sun, L., & Chang, C. (2019). Rotation effect of flexible wheelset on wheel-rail force in Euler coordinate system. *China Railway Science*, *40*(4), 120–128.

Gao, H., Dai, H., & Ni, P. (2012). Algorithm of wheel-rail contact point for flexible wheelset. *Journal of The China Railway Society*, *34*(5), 26–31.

Han, P., & Zhang, W. (2015). Influences of structural bending deformation and profile wear of wheelsets on vibration performance of high-speed trains. *Journal of Vibration and Shock*, *34*(5), 207–212.

Han, J., Zhong, S., Xiao, X., Wen, Z., Zhao, G., & Jin, X. (2018). High-speed wheel/rail contact determining method with rotating flexible wheelset and validation under wheel polygon excitation. *Vehicle System Dynamics*, *56*(8), 1233–1249. doi: 10.1080/00423114.2017.1408920.

Hu, X., Hou, Y., Song, Z., Cheng, D., & Hou, M. (2018). Simulation study on influence of harmonic wear of wheel on vibration of high-speed wheel-rail system based on flexible wheel-rail model. *China Railway Science*, *39*(6), 29830. doi: 10.3969/j.issn.1001-4632.2018.06.11.

Hussein, B., & Shabana, A. (2011). Sparse matrix implicit numerical integration of the stiff differential/algebraic equations: Implementation. *Nonlinear Dynamics*, *65*(4), 369–382. doi: 10.1007/s11071-010-9898-9.

Kan, Z., Peng, H., & Chen, B. (2017). Rigid body system dynamic with the accurate Jacobian matrix of spring-damper-actuator. *Chinese Journal of Theoretical and Applied Mechanics*, *49*(5), 1103–1114.

Ma, C., Gao, L., Xin, T., Cai, X., Nadakatti, M., & Wang, P. (2021). The dynamic resonance under multiple flexible wheelset-rail interactions and its influence on rail corrugation for high-speed railway. *Journal of Sound and Vibration*, *498*, 115968. doi: 10.1016/j.jsv.2021.115968.

Momhur, A., Zhao, Y., Quan, L., Sun, Y., & Zou, X. (2021). Flexible-rigid wheelset introduced dynamic effects due to wheel tread flat. *Shock and Vibration*, *2021*, 1–21. doi: 10.1155/2021/5537286.

Song, Z., Hou, Y., Hu, X., Zhang, H., Li, Q., & Cheng, D. (2018). Research on vibration characteristics of wheel-rail corrugation under flexible wheel and rail. *Journal of the China Railway Society*, *40*(11), 33–40. doi: 10.3969/j.issn.1001-8360.2018.11.005.

Sun, L., Ai, J., Gao, R., Zhang, L., & Cui, S. (2023). Influence of flexible wheelset and wheel polygon on dynamic response of wheel-rail system of high speed railway. *China Railway*, *2023*(5), 104–110.

Wu, X., Rakheja, S., Ahmed, A., & Chi, M. (2018). Influence of a flexible wheelset on the dynamic responses of a high-speed railway car due to a wheel flat. *Proceedings of the Institution of Mechanical Engineers, Part F. Journal of rail and rapid transit*, *232*(4), 1033–1048). doi: 10.1177/0954409717708895.

Yang, G., & Ren, Z. (2018). Wheel/rail contact performance on curved track of high-speed EMU with elastic model. *Journal of Mechanical Engineering*, *54*(4), 132–141. doi: 10.3901/jme.2018.04.132.

Zeng, Y., Wen, B., Yu, W., Cheng, L., & Wang, C. (2012). Calculation and research on wheel-rail 3D contact geometry based on projection contour. *China Railway Science*, *33*(6), 51–59.

Zhang, B., Lu, Z., & Wang, H. (2013). Analysis on wheel-rail contact parameters of elastic wheelset. *Journal of Tongji University (Natural Science)*, *41*(4), 577–582.

Zhong, S., & Jin, X. (2017). The influence of rotating effect of wheelset and structural flexibility on wheel-rail force. In *Chinese Mechanics Conference-Collected Papers from the 2017 Celebration of the 60th Anniversary of the Founding of the Chinese Society of Mechanics*, Beijing (pp. 1075–1084).

387

Corresponding author
Lixia Sun can be contacted at: lxsun@live.com